ADVANCES IN ATMOSPHERIC SCIENCES, VOL. 38, JULY 2021, 1238–1251

• **Original Paper** •

Smog Chamber Study on the Ozone Formation Potential of Acetaldehyde

Hailiang ZHANG[1,2], Yongfu XU[*1,2], Long JIA[1,2], and Min XU[1,2]

[1]*State Key Laboratory of Atmospheric Boundary Layer Physics and Atmospheric Chemistry*, *Institute of Atmospheric Physics*, *Chinese Academy of Sciences*, *Beijing* 100029, *China*

[2]*Department of Atmospheric Chemistry and Environmental Sciences*, *College of Earth and Planetary Sciences*, *University of Chinese Academy of Sciences*, *Beijing* 100049, *China*

(Received 27 November 2020; revised 24 March 2021; accepted 8 April 2021)

ABSTRACT

Acetaldehyde is one of the important VOC species of O_3 precursors in the atmospheric environment. The influences of relative humidity (RH) and initial VOC/NO_x ratio (R_{CN}) on the formation of O_3 are studied in smog chamber experiments, and the MCM v3.3.1 mechanism of acetaldehyde is modified based on the experimental results. In low-RH conditions (RH = 11.6%±1.1%), the O_3 concentration at 6 h increases first and then decreases with the increase of R_{CN}, and the R_{CN} at the inflection point of O_3 concentrations is 3.2. In high-RH experiments (RH = 78.8%±1.0%), variation of the O_3 concentration at 6 h with R_{CN} is similar to that in low-RH experiments, but the R_{CN} at the inflection point is 2.8. RH has no significant effect on the O_3 concentrations under low R_{CN} (< 3), whereas it has a negative effect under high R_{CN} (> 3). Compared with the experimental results, original MCM v3.3.1 greatly underestimates the O_3 concentrations. Addition of both the photolysis process of peroxyacetyl nitrate and the photolysis process of HNO_3 on the reactor surface into the original MCM can reduce the difference between the simulated O_3 concentrations and the experimental results at 6 h from 24%–35% and 17%–49% to 6%–26% and 10%–42% under low- and high-RH conditions, respectively. The maximum incremental reactivity (MIR) of acetaldehyde simulated with the modified MCM is 4.0 ppb ppb^{-1} without considering the effect of other VOCs.

Key words: ozone, acetaldehyde, photochemical reaction, MCM

Citation: Zhang, H. L., Y. F. Xu, L. Jia, and M. Xu, 2021: Smog chamber study on the ozone formation potential of acetaldehyde. *Adv. Atmos. Sci.*, **38**(7), 1238–1251, https://doi.org/10.1007/s00376-021-0407-5.

1. Introduction

Ozone (O_3) is an important pollutant in the troposphere, especially in the urban atmosphere, which affects the quality of atmospheric environment (Dong et al., 2020; Kinose et al., 2020) and human health (Liang et al., 2020; Zhao et al., 2020). In the past few decades, ozone has received considerable attention (Carter et al., 1993; Derwent et al., 2007; Wang et al., 2017; Cao et al., 2020).

In recent years, although a series of control measures for air pollution have been formulated and implemented in various places, ozone pollution incidents still occur frequently (Chi et al., 2018; Ma et al., 2019; Guérette et al., 2020; Janik et al., 2020; Kalabokas et al., 2020; Seltzer et al., 2020). In the Beijing–Tianjin–Hebei region, the Yangtze River Delta, and the Pearl River Delta of China, air pollution events with ozone concentration exceeding 100%–200% of the air standard value have been observed many times (Wang et al., 2017). Cao et al. (2020) observed that the ozone concentration in the west China rain zone and its adjacent regions has exceeded the relevant ecological critical loads. In Sydney, Australia, the ozone concentration can even exceed 100 ppb when ozone pollution occurs (Guérette et al., 2020). Seltzer et al. (2020) found that the harmful impacts of long-term exposure to ambient ozone on human health increased from 2000 to 2015 in USA.

O_3 precursors are volatile organic compounds (VOCs) and nitrogen oxide (NO_x). Among thousands of VOCs species, carbonyl compounds such as aldehydes and ketones are considered to be the important precursors of ozone formation (Dong et al., 2014; da Silva et al., 2016). It is known that acetaldehyde, as one of the main carbonyl compounds, has a significant effect on the formation of ozone (Saengsai and Jinsart, 2015). Guo et al. (2014) found that acetaldehyde contributed 42% of the total carbonyl compounds to

* Corresponding author: Yongfu XU
Email: xyf@mail.iap.ac.cn

the summer ozone concentration in the rural areas of Southern China, while da Silva et al. (2016) found that acetaldehyde was the most important precursor of ozone in Rio de Janeiro as compared with other carbonyls such as formaldehyde and aromatics such as benzene and toluene. In fact, its contribution to local ozone was about 2.6 times that of formaldehyde.

Many chemical mechanisms have been widely used to simulate ozone formation (Shi et al., 2012), such as Master Chemical Mechanism (MCM) (Jenkin et al., 1997, 2003, 2015) and Statewide Air Pollution Research Center mechanism (SAPRC) (Carter and Heo, 2013; Venecek et al., 2018). It is often found that there are some differences in the simulation results between different chemical mechanisms (Zong et al., 2018). To improve the accuracy of simulation results, it is necessary to evaluate and improve the chemical mechanisms according to experimental results (Derwent et al., 1998; Carter and Heo, 2013; Zong et al., 2018). Carter and Heo (2013) have supplemented the SAPRC mechanism many times, and the MCM mechanism has also been modified in some studies (Jia et al., 2009; Jia and Xu, 2016). To the best of our knowledge, the only known experimental study on the ozone formation of acetaldehyde was carried out by Carter et al. (1993), whose purpose was to verify the accuracy of the simulation result of SAPRC. Their experiments mainly focused on the influence of effective light intensity under low relative humidity (~15%). Smog chamber experiments regarding the influences of relative humidity (RH) and precursor concentrations on ozone formation from the photochemical reaction of acetaldehyde have not been reported in detail. Also, whether the MCM mechanism can accurately simulate the reaction process under different reaction conditions remains to be evaluated by experiments.

In this study, the ozone formation potential of acetaldehyde is studied in detail through the smog chamber system. The main research purposes are as follows: (1) to determine the influence of initial CH_3CHO/NO_x ratios (R_{CN}) on ozone concentrations under different RHs, (2) to evaluate whether the current known chemical mechanism (MCM) can accurately simulate the photochemical reaction of acetaldehyde, and (3) to estimate the influence of acetaldehyde on the ozone concentrations in the real atmospheric environment.

2. Experimental and Simulation details

2.1. *Experimental details*

All experiments in this study were carried out in a smog chamber system. The detailed description of this smog chamber system has been given in our previous studies (Jia and Xu, 2016, 2018). The reactor has a volume of 1.3 m^3 in this study. The light source was supplied by two types of UV lamps F40 BLB (GE, USA) and UVA-340 (Q-Lab Corporation, USA), with center wavelengths of 365 nm and 340 nm, respectively. These types of UV lamps have been used in other similar studies to simulate the sunlight in the real atmospheric environment (Wang et al., 2015; Luo et al., 2019, 2020; Chen et al., 2020). The NO_2 photolysis rate constant was determined to be $J[NO_2] = 0.20\ min^{-1}$ to represent the effective light intensity in the reactor, which is in the range of 0.139–0.44 min^{-1} widely used in other similar photochemical reaction systems such as 1,2,3-trimethylbenzene-NO_x (Luo et al., 2019), toluene-NO_x (Chen et al., 2020), and styrene-NO_x (Luo et al., 2020).

The background air used in all experiments was zero air produced by the Zero Air Supply (Model 111 and Model 1150, Thermo Scientific, USA), in which the concentrations of O_3, NO and NO_x are below 1 ppb, and the concentrations of SO_2 and hydrocarbon (HC) are below 50 ppt and 100 ppb, respectively. The concentration of the NO_2 standard gas was 508 ppm (diluted by N_2, Beijing Huayuan Gas Co., Ltd., China). The purity of acetaldehyde was 99.9% (Aladdin Reagent Co., Ltd., China). The RH of background air was controlled by bubbling zero air through the highly purified water. A hygrometer (Model 645, Testo AG, Germany) was used to measure temperature and RH in the experiments, with the accuracy being ±0.1°C and ±1%RH. The concentrations of NO_x (NO and NO_2) and O_3 were measured online by a NO_x analyzer (Model 42C, Thermo Scientific, USA) and an O_3 analyzer (Model 49C, Thermo Scientific, USA), respectively. The concentration of NO_2 measured by the NO_x analyzer included all other nitrogen-containing substances (NO_2, HNO_3, etc.) except NO, which is expressed as NO_y below. The concentration of acetaldehyde was measured by GC-MS (7890A/5975, Agilent, USA).

Before each experiment, the reactor was flushed with zero air with the light on until the concentrations of NO, NO_y and O_3 in the reactor were all lower than the detection limit of the instruments (1 ppb). A solenoid valve was used to control the flow of the background air into the reactor. When the background air filled half of the volume of the reactor, acetaldehyde was introduced into the reactor with zero air through the tee on the intake pipe, and the NO_2 standard gas was directly injected from the sample inlet of the reactor with a special syringe. After the reactor was full, the reactor was left for 0.5 h under the condition of no light and no activity, and then the initial condition in the reactor, including the temperature of the reactor and the initial concentrations of NO, NO_2, O_3 and acetaldehyde, was determined. After the measurement of the initial condition, the light was immediately turned on, marking the beginning of the experiment. During the experiment, the temperature around the reactor was kept stable (±1°C). The experimental initial conditions are shown in Table 1. Experiments 1–8 are used to study the effect of the ratio of initial CH_3CHO concentrations to NO_x concentrations ($NO_x = NO + NO_2$) on ozone concentrations under low-RH (10.7%–13.5%), while Experiments 9–14 are used for high–RH conditions (77.5%–79.8%). Hereafter, the ratio of initial CH_3CHO concentrations to NO_x concentrations is termed R_{CN}. The variation of R_{CN} was mainly realized by changing initial NO_x concentrations under the fixed initial CH_3CHO concentrations.

Because the ozone concentration at 6 h in the photochemical reaction was generally used to represent the actual ozone formation ability of VOC (Carter et al., 1993), an experiment in this study lasted for 6 h.

2.2. *Simulation details*

In order to evaluate the accuracy of the MCM mechanism regarding the photochemical reaction of acetaldehyde, the results from the smog chamber experiments were compared with the simulated results by using MCM v3.3.1 (Jenkin et al., 2015). In the simulation of MCM v3.3.1, the wall loss rates of NO_x, O_3, acetaldehyde, formaldehyde, etc. were taken into account, and the source of HONO from NO_2 was also included. In addition to these chamber-dependent reaction processes and species, the mechanism of the photochemical reaction of acetaldehyde in MCM v3.3.1 included 136 chemical reactions and 46 species (http://mcm.leeds.ac.uk/mcmv3.3.1/). To solve these many ordinary differential equations and run the kinetic model under MATLAB, a chemical reaction compiler (CRC) developed by Jia (2007) was used to automatically generate MATLAB code for the simulation of the kinetic processes of the chamber experiments. A variable-order solver soft package called ode15s in MATLAB was used.

Table 1. Initial conditions in the CH_3CHO-NO_x experiments. ([a]: Initial concentrations of CH_3CHO were calculated based on the injected volume of acetaldehyde regent.).

Expts. No.	CH_3CHO (ppm)	NO_x (ppb)	RH (%)	T (K)	R_{CN}
1	0.62	539.0	12.7	299.0	1.1
2	0.65	325.0	10.9	299.2	2.0
3	0.65	191.0	10.7	299.2	3.4
4	0.60 [a]	131.2	12.0	300.8	4.6
5	0.64	87.4	10.7	301.3	7.3
6	0.69	75.4	11.5	301.0	9.2
7	0.60	57.2	13.5	300.3	10.4
8	0.60	43.7	11.4	301.0	13.7
9	0.66	506.0	77.5	300.4	1.3
10	0.65	345.0	78.0	299.7	1.9
11	0.57	187.5	79.8	298.8	3.0
12	0.65	96.8	78.3	298.8	6.7
13	0.68	87.9	79.4	299.8	7.7
14	0.61	46.9	79.8	299.2	13.0

3. Results and discussion

3.1. *Results from smog chamber experiments*

Figure 1 shows variations of O_3, NO_y, NO and CH_3CHO concentrations with time from the experiments under different RHs and initial reactant concentration ratios. The growth rate of O_3 concentrations is the largest in the first 1–2 minutes from the start of the experiment (Fig. 1a).

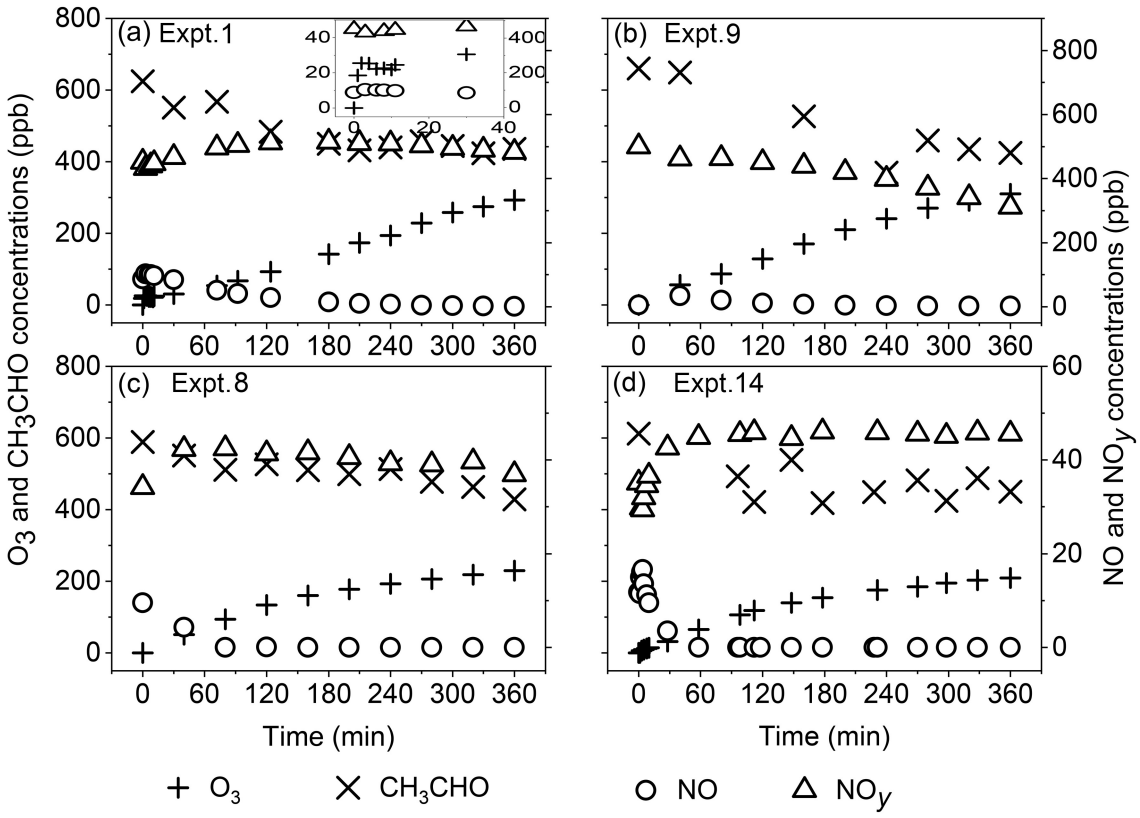

Fig. 1. Variations of measured concentrations of O_3, NO, NO_y and CH_3CHO in the reactions with time under different RHs (a: 12.7%; b: 77.5%; c: 11.4%; d: 79.8%) and R_{CN} (a: 1.1; b: 1.3; c: 13.7; d: 13.0) (No wall loss correction for all concentrations).

After that, the O_3 concentration maintains a rapid increasing trend, which is due to formation of RO_2 radicals generated from the photochemical reaction of CH_3CHO. Because of the photolysis of NO_2, the concentration of NO increases rapidly and NO_y decreases rapidly within the first 1–2 minutes. Then, the NO concentration decreases gradually, and meanwhile, the NO_y concentration increases slowly, which is due to the gradual conversion of NO to nitrogen-containing substances such as NO_2 and peroxyacetyl nitrate (PAN). However, due to the effect of wall losses, there is a decreasing trend of NO_y in the later stage of reactions. The CH_3CHO concentration decreases rapidly at the beginning of reactions, but the decreasing rate gradually becomes smaller in the later stage of most experiments.

The photochemical reaction process is significantly affected by light intensity, temperature, RH, reactant concentrations, etc. In this study, the impacts of the initial reactant concentration ratio R_{CN} and RH on the photochemical reaction of acetaldehyde were the primary foci of interest, and only these results are reported herein.

3.1.1. *Impacts of initial concentration ratios on O_3*

R_{CN} has a significant effect on NO_y, for which the different R_{CN} effects can be seen under different RH conditions (Fig. 1). Under low-RH conditions, R_{CN} greatly affects the increase rate of NO_y in the early stage of the reaction. The time required for the NO_y concentration to reach its maximum value in Expt. 8 (R_{CN} = 13.7, RH = 11.4%) is about 80 minutes earlier than that in Expt. 1 (R_{CN} = 1.1, RH = 12.7%). However, under high-RH conditions, R_{CN} mainly affects the pattern of the variation of NO_y with time. In Expt. 9 (R_{CN} = 1.3, RH = 77.5%), the NO_y concentration decreases almost linearly with time after the start of reactions, while in Expt. 14 (R_{CN} = 13.0, RH = 79.8%) it increases during the first one hour of reactions, and then becomes essentially unchanging. At the same RH conditions, the conversion rate of NO_x is different under different R_{CN}, which leads to the difference of the concentrations of chemical components in NO_y. In addition, the rate of conversion of NO_2 to HONO under different RHs is significantly different (Hu et al., 2011), and the different wall loss rate of NO_2 under different RHs was also observed (Jia et al., 2011). These are probably the reasons for the influence of R_{CN} and RHs on the NO_y concentrations.

The R_{CN} also has a significant impact on the O_3 concentration during the experiment. Under the condition of R_{CN} = 1.1 in Expt. 1 (Fig. 1a), the average formation rate of O_3 is about 0.79 ppb min^{-1} in the first 180 minutes, which is close to 0.83 ppb min^{-1} during the second 180 minutes from time t = 180–360 minutes. However, under the condition of R_{CN} = 13.7 in Expt. 8 (Fig. 1c), the average formation rate of O_3 is about 1.00 ppb min^{-1} in the first 180 minutes, but it is only 0.35 ppb min^{-1} during the later stage of 180 minutes from t = 180–360 minutes. Similarly, the average formation rate of O_3 in Expt. 9 (R_{CN} = 1.3) does not change significantly during the first and second 180 minutes of the experiment, while in Expt. 14 (R_{CN} = 13.0) it is larger in the first 180 minutes than in the second 180 minutes. With the increase of R_{CN}, the concentration of NO_2 decreases. Therefore, under high R_{CN}, such as Expts. 8 and 14, the low concentration of NO_2 reduces the increase of the formation rate of O_3 at the later stage of reactions.

Variation of the O_3 concentration with R_{CN} at time t = 6 h is shown in Fig. 2. Under low-RH conditions (Expts. 1–8), with the increase of R_{CN} from 1.1 to 3.4, the O_3 concentration at t = 6 h increases rapidly, while the O_3 concentration at t = 6 h decreases rapidly with the increase of R_{CN} in the range of 4.6–13.7. According to the variation pattern of O_3 concentration with R_{CN} in Expts. 1–8 in Fig. 2, it is estimated that the R_{CN} at the inflection point of the curve that describes variation of O_3 concentrations with R_{CN} is 3.2. Similarly, under high-RH conditions, the fitting result of R_{CN} for Expts. 9–14 is 2.8 at the inflection point.

3.1.2. *Impacts of RH on O_3*

It is known from Fig. 2 that the effect of RH on the O_3 concentration at 6 h is different under different R_{CN}. On the left side of the O_3 inflection point (R_{CN} < 3), there is no significant difference in the O_3 concentration at 6 h between low and high RHs. As R_{CN} rises, the difference increases. When R_{CN} > 4.6, the O_3 concentration at 6 h under high RH is about 16% lower than that under low RH on average. Under low R_{CN} (R_{CN} on the left side of the O_3 inflection point), the wall loss rate of O_3 increases under high RH, but the increase in the loss of NO_2 on the reactor surface can promote the formation of O_3. Thus, the RH effect on the O_3 concentration is generally limited. However, under high R_{CN} (R_{CN} on the right side of the O_3 inflection point), the increase of NO_2 wall loss under high RH will further reduce the O_3 formation. As a result, the O_3 concentration under high RH is lower than that under low RH.

RH can also affect the amount of acetaldehyde con-

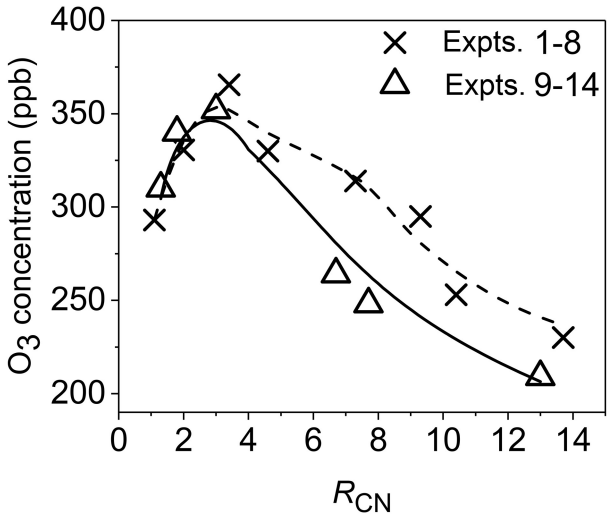

Fig. 2. Variations of the O_3 concentration at time t=6 h with R_{CN} under different RHs (11.6%±1.1% in Expts. 1–8, 78.8%±1.0% in Expts. 9–14; the symbols represent experimental values, and the dashed and solid lines represent fitting results of Expts. 1–8 and Expts. 9–14, respectively).

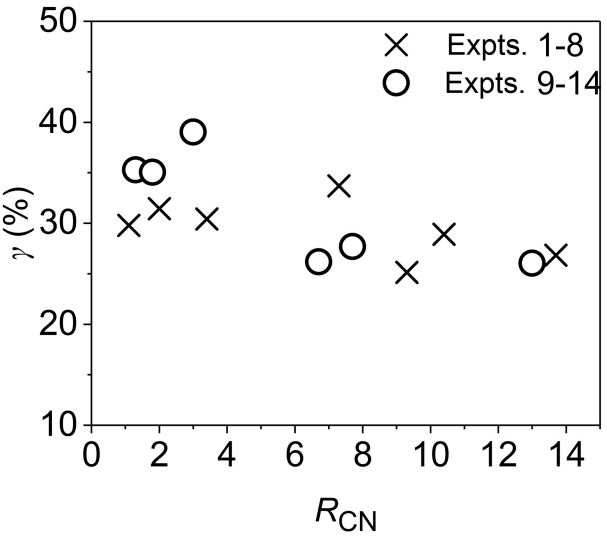

Fig. 3. Variations of proportion (γ) of CH_3CHO consumed in the reactions with R_{CN}.

sumed in the reaction. According to the change of CH_3CHO concentrations, the proportion (γ) of CH_3CHO that participated in the reaction at the end of each experiment (the ratio of CH_3CHO consumed at the end of an experiment to its initial concentration) was calculated and is plotted against R_{CN} in Fig. 3. In the low-RH experiments (Expts. 1–8), the values for γ range from 25% to 33% under the different R_{CN}, for which γ is 31% and 29% on average under $R_{CN} \leqslant 3.4$ and $R_{CN} \geqslant 4.6$, respectively. However, in the high-RH experiments (Expts. 9–14), under $R_{CN} \leqslant 3.0$, the average value of γ is 36%, which is higher than that under $R_{CN} \geqslant 6.7$ (27%). Under low R_{CN}, the initial concentration of NO_2 was larger than that under high R_{CN}, which generated higher HONO concentrations and OH radical concentrations. This is a main reason for larger consumption of acetaldehyde under low R_{CN}.

3.1.3. *Incremental reactivity (IR) of CH_3CHO*

In order to further study the formation of O_3 from CH_3CHO, the incremental reactivity (IR) of acetaldehyde is calculated using the following formula (Carter et al., 1995):

$$\mathrm{IR}[\Delta(\mathrm{O_3{-}NO})]_{t,\mathrm{VOC}} = \frac{\Delta \mathrm{O_3{-}NO}_{t,\mathrm{test}} - \Delta \mathrm{O_3{-}NO}_{t,\mathrm{blank}}}{[\mathrm{VOC}]_0}, \quad (1)$$

where $\Delta(\mathrm{O_3{-}NO})_{t,\mathrm{test}}$ is $([\mathrm{O_3}]_t{-}[\mathrm{NO}]_t){-}([\mathrm{O_3}]_0{-}[\mathrm{NO}]_0)$ measured at time t from the start of an experiment where the test VOC is added, $\Delta(\mathrm{O_3{-}NO})_{t,\mathrm{blank}}$ is the corresponding value from the experiment where the test VOC is not present, and $[\mathrm{VOC}]_0$ is the amount of test VOC added. Taking Expt. 2 as an example, we see that IR shows a strongly increasing trend with reaction time (Fig. 4a) until the end of the experiment (6 h). Similar changes in IR from other experiments are also seen, which is probably due to the presence of PAN as the reservoir of NO_x in the reaction, leading to the time lag to reach the maximum O_3 concentration. From the comparison of Expt. 2 (RH = 10.9%) with Expt. 10 (RH = 78.0%), it is found that RH has little effect on IR during the experiment, and the IR at the end of the experiment (6 h) in Expt. 2 is about 5% larger than that in Expt. 10. Similarly, for Expts. 8 and 14, RH generates a 12% difference in IR between these two experiments (Fig. 4a). However, the comparison of Expts. 2 (R_{CN} = 2.0) and 8 (R_{CN} = 13.7) shows that R_{CN} has an effect on IR, and the IR at 6 h (IR_{6h}) from Expt. 2 is about 1.8 times that from Expt. 8. The variation of IR_{6h} under different R_{CN} is shown in Fig. 4b. This indicates that under different RH conditions, the IR_{6h} is larger under low R_{CN} than under high R_{CN}. Under high R_{CN}, the low concentration of NO_2 is not conducive to the formation of ozone, which is consistent with the small amount of CH_3CHO consumed. In addition, the IR_{6h} under high RH is lower than that under low RH, which is consistent with the variation of O_3 concentrations under different RH conditions. The wall loss rate of O_3 increases with increasing RH,

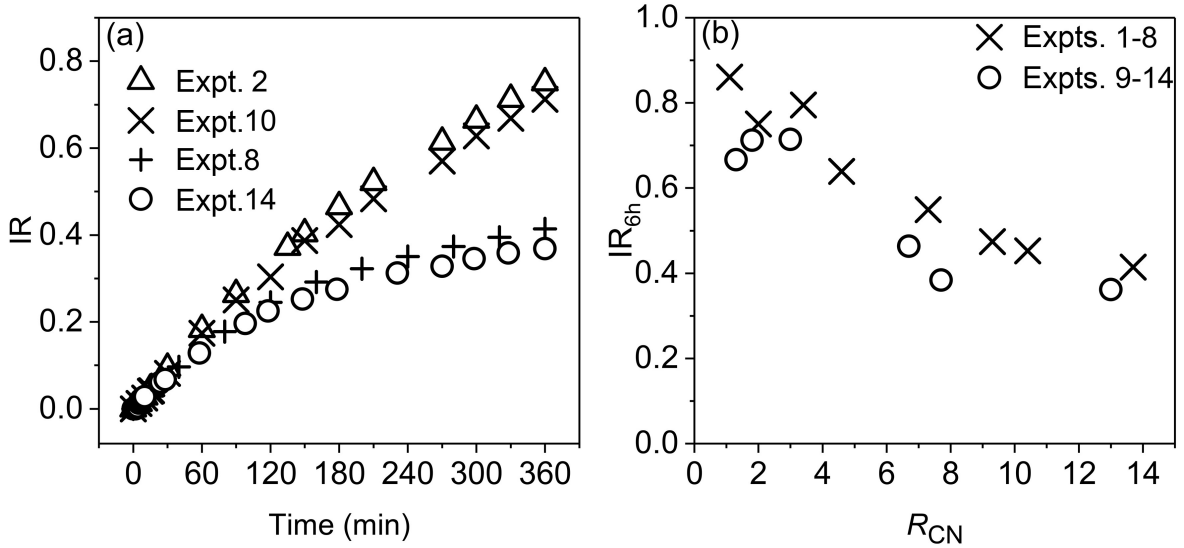

Fig. 4. Variations of experiment-based incremental reactivity (IR) of acetaldehyde with time (a), and IR_{6h} with R_{CN} (b).

which leads to a decrease in IR. Besides, the wall loss rate of NO_2 also increases with the increase in RH, which further reduces the O_3 formation under high R_{CN}, leading to great reduction of the IR of acetaldehyde.

3.2. *Simulated results*

3.2.1. *Evaluation of MCM v3.3.1 with experimental results*

MCM v3.3.1 was used to simulate the concentrations of NO, NO_y, CH_3CHO and O_3 in Expts. 1–14. The simulation from the original MCM mechanism and relevant auxiliary reactions (mainly wall losses) is named Run1 below.

Compared with the measured O_3 concentrations, the simulated results from Run1 are underestimated under different RH conditions. Taking Expts. 2 and 10 as examples (Fig. 5), we see that the differences in the O_3 concentration between the simulations and experiments increase with the reaction time. As a result, the simulated O_3 concentrations at the end of experiments (6 h) are 29% and 49% lower than the measured concentrations in Expts. 2 and 10, respectively. Further analysis shows that the maximum difference between the simulated and measured O_3 concentrations at the end of experiments appears to be at the inflection point of the curve that describes variation of O_3 concentrations with R_{CN} (Figs. 6a and 6b). Meanwhile, it should be noted from Figs. 6a and 6b that under both low and high RHs, the R_{CN} values at the inflection point of O_3 concentrations at 6 h differ greatly between the experiments and simulations. For Expts. 9–14 with high RH, the experimental O_3 concentration at 6 h reaches a maximum at R_{CN} = 3.0 (Expt. 11), while the simulated O_3 concentration reaches the maximum at R_{CN} = 7.7 (Expt. 13). Thus, the simulated O_3 concentration at 6 h for the R_{CN} of 3.0 (Expt. 11) is 49% lower than the observed value, while for the R_{CN} of 7.7 (Expt. 13) the simulated value is only 17% lower than the observed one. Similarly, for Expts. 1–8 with low RH, the experimental O_3 concentration at 6 h reaches a maximum at R_{CN} = 3.4 (Expt. 3), while the simulated value reaches the maximum at R_{CN} = 4.6 (Expt. 4), leading to the maximum difference between the simulated and measured O_3 concentrations appearing at R_{CN} = 3.4 (Expt. 3).

It can be concluded that when $R_{CN} \leqslant 3.4$, the difference in the O_3 concentration at 6 h between simulations and experiments in the high-RH experiments (48% ± 1%) is larger than that in the low-RH experiments (29% ± 6%), while when $R_{CN} \geqslant 4.6$, this difference in the high-RH experiments (23%±5%) is smaller than that in the low-RH experiments (29% ± 1%).

Run1 simulates well the variation of the experimental NO concentration, although the simulated concentration is higher than the measured value, which is consistent with the underestimation of O_3 in Run1. Meanwhile, Run1 simulates well the variation of NO_y with time (Fig. 5), with the largest difference between the simulated and measured values mainly appearing at the end of the experiments (6 h) as a whole, as shown in Figs. 6c and 6d. The differences in the NO_y concentration at 6 h between the simulations and experiments are generally less than 20% except for Expt. 9 (41%) and Expt. 10 (38%). Under high-RH conditions, the effect of wall losses on NO_y was probably large, and at the same time, the NO_y concentration decreased with increasing R_{CN}. Combination of high RH and low R_{CN} generates the large difference in NO_y for Expts. 9 and 10.

The difference between the measured and simulated CH_3CHO concentrations is relatively smaller than that for other chemical components, with the largest difference appearing at the end of Expt. 1, in which the simulated result is 31% lower than the measured result (Figs. 6e and 6f). Nevertheless, under low- and high-RH conditions, the differences between the simulated and measured CH_3CHO concentra-

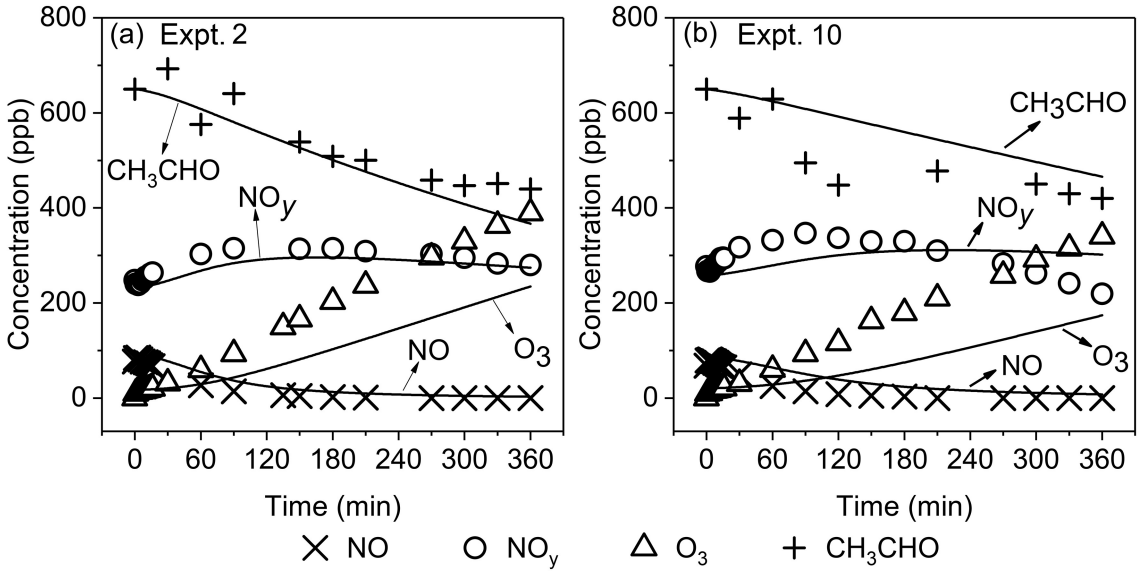

Fig. 5. Variations of simulated and measured concentrations of NO, NO_y, O_3 and CH_3CHO (Symbol in the figure represents experimental observation values, and solid line represents simulated values by MCM v3.3.1).

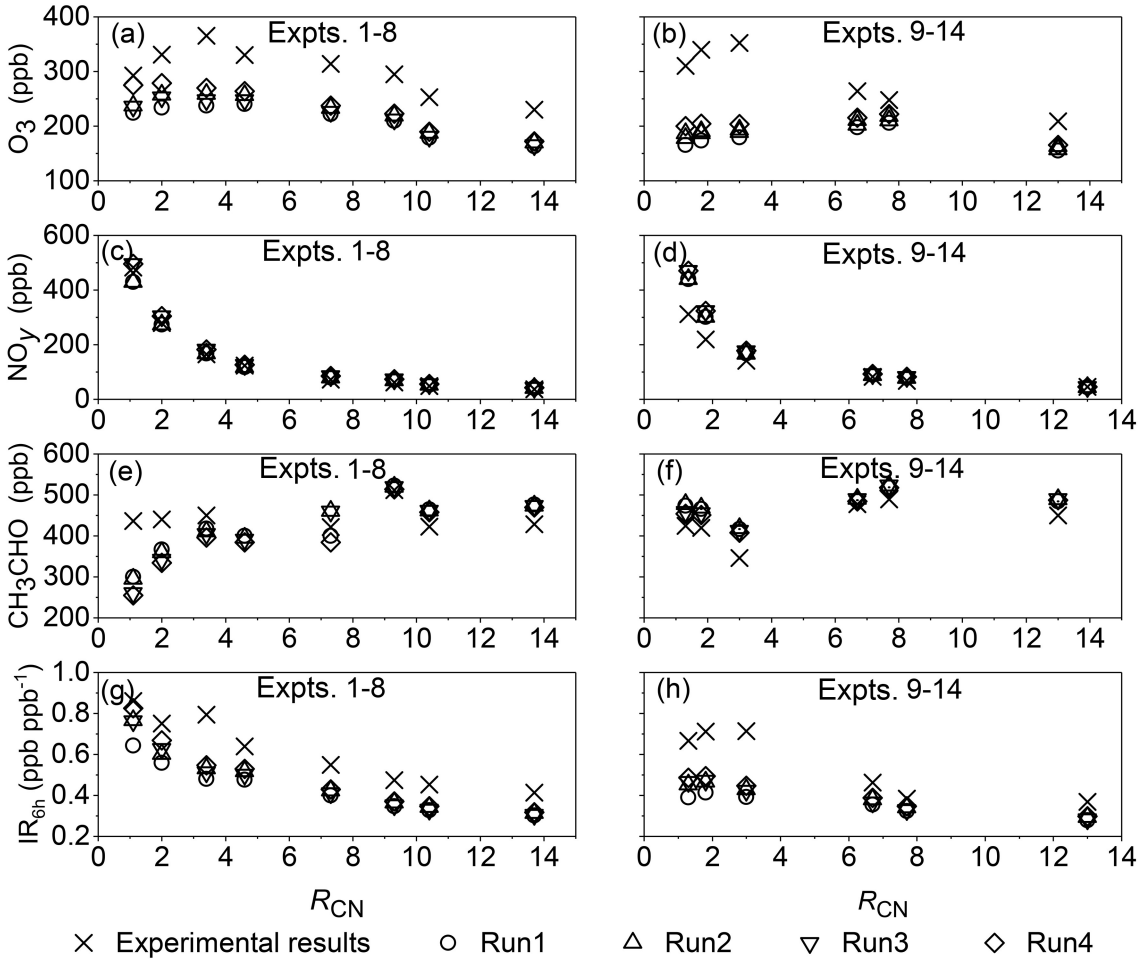

Fig. 6. Comparison of simulated and measured concentrations of O_3, NO_y, CH_3CHO and IR_{6h} at the end of experiments from different cases (Run1: original MCM v3.3.1; Run2: MCM v3.3.1 with R1; Run3: MCM v3.3.1 with R2; Run4: MCM v3.3.1 with R1 and R2).

tions at the end of the experiments are 12% ± 10% and 9% ± 7% on average, respectively. In addition, in the low-RH experiments (Expts. 1–8), the simulated acetaldehyde concentration at 6 h gradually varies from underestimate to overestimate, while in the high-RH experiments (Expts. 9–14), all Run1-simulated results are slightly larger than the experimental results. The simulation of CH_3CHO can be affected by the simulation of NO_y. For example, when Run1-simulated results underestimate the experimental concentrations of NO_y under low R_{CN}, the reaction between OH radical and acetaldehyde is generally enhanced, which leads to the underestimation of the acetaldehyde concentration, whereas under high R_{CN}, the overestimation of NO_y can promote the formation of OH radicals, which also can lead to the underestimation of acetaldehyde.

It is known that the accuracy of Run1-simulated results for different species is different in the photochemical reaction of acetaldehyde, and the accuracy of simulated results is closely related to the reactant concentration and RH. Therefore, for the verification of the accuracy of different mechanisms for the photochemical reaction of acetaldehyde, the influence of reaction conditions should be fully considered.

3.2.2. *Evaluation of MCM with IR*

The simulated IR value of acetaldehyde at the end of experiments (6 h) by MCM v3.3.1 is lower than the experiment-based value (Figs. 6g and 6h), with the underestimated values being 28% ± 5% in Expts. 1–8 and 32% ± 12% in Expts. 9–14, respectively. In the low-RH experiments (Expts. 1–8) both the simulated and experiment-based IR_{6h} values decrease with increasing R_{CN}, while in the high-RH experiments (Expts. 9–14), the experiment-based IR_{6h} varies non-monotonically with increasing R_{CN}, but the simulated IR_{6h} varies steadily as a whole. It is known that high RH accentuates the difference in IR_{6h} between MCM and experiments. This further demonstrates that the mechanism of the photochemistry of acetaldehyde in MCM v3.3.1 probably needs to be improved.

3.2.3. *Improvement of the MCM mechanism of acetaldehyde*

In the simulation results from Run1, the NO_y concentration includes the PAN concentration, which can account for about 80% of the NO_y concentration at the end of the experiments. Because there are some differences in the NO_y concen-

tration between the Run1-simulated and experimental results, it is considered that the reaction process of PAN is probably important for improving the simulation.

The removal process of PAN in the real atmospheric environment mainly includes its reaction with OH radicals, pyrolysis process and photolysis process (R1) (Seinfeld and Pandis, 2006). It is considered that the atmospheric loss rate of PAN by photolysis is greater than that by its reaction with OH radicals, and when altitude is > 7 km from the ground, the loss rate of PAN by photolysis is even larger than that by pyrolysis (Talukdar et al., 1995).

Many researchers have investigated the photolysis process of PAN (Libuda and Zabel, 1995; Talukdar et al., 1995; Flowers et al., 2007). With the further understanding of the photolysis process of PAN, the influence of photolysis processes on the loss of PAN has been gradually realized in the photochemical reaction of acetaldehyde. In the earlier version (SAPRC-99) of the SAPRC mechanism, the photolysis process of PAN (R1) was ignored. This process was included for the first time in version SAPRC-07 (Carter, 2010), and it is also used in the latest version of SAPRC-11 (Carter and Heo, 2013). The photolysis rate constant adopted was $k_1 = 6.12 \times 10^{-5}$ cm^3 molecule^{-1} s^{-1} (300 K). Nevertheless, only the reaction of PAN with OH radicals and its pyrolysis have been included in MCM v3.3.1, while the photolysis of PAN has not yet been included.

$$\mathrm{PAN}+h\nu \rightarrow 0.6\left(\mathrm{CH_3CO_3}+\mathrm{NO_2}\right)+ 0.4\left(\mathrm{CH_3O_2}+\mathrm{CO_2}+\mathrm{NO_3}\right). \quad \text{(R1)}$$

In order to determine the influence of R1 on the photochemical reaction of acetaldehyde in this study, R1 was added to original MCM v3.3.1, and $k_1 = 6.12 \times 10^{-5}$ cm^3 molecule^{-1} s^{-1} was also used in the simulation, but the influence of temperature difference between different experiments is ignored. The smog chamber experiments in this study were re-simulated, which is named Run2 below.

The simulated O_3 concentrations at time t = 6 h from Run2 are shown in Figs. 6a and 6b. Compared with Run1, the simulated O_3 concentrations at 6 h in Expts. 1–8 and Expts. 9–14 in Run2 increased by 4%–10% and 5%–8%, respectively. Also, the increased amount for $R_{CN} \leqslant 3.4$ (8.3% ± 2.1% for Expts. 1–8 and 7.7% ± 0.2% for Expts. 9–14) is larger than that for $R_{CN} \geqslant 4.6$ (5.1% ± 0.9% and 6.0% ± 0.9%). In Expts. 1–8 and Expts. 9–14, the average differences between the Run2-simulated and measured NO_y concentrations at 6 h are 3% ± 9% and 19% ± 17%, respectively, which are close to those between the Run1-simulated and measured results (4% ± 9% and 20% ± 17%) (Figs. 6c and 6d). Similarly, the average differences between the Run2-simulated and measured CH_3CHO concentrations at 6 h are 4% ± 16% and 11% ± 6% for Expts. 1–8 and Expts. 9–14, which are also close to those between Run1 and experimental results (5% ± 15% and 10% ± 6%) (Figs. 6e and 6f). Because of the competitive reactions of PAN and CH_3CHO with OH radicals, adding R1 to MCM will lead to the increase of OH radical concentrations, which will slightly increase the amount of CH_3CHO consumed in the reactions and promote the formation of O_3. For example, compared with the simulation results for Expt. 2 in Run1, the OH radical concentration at 6 h in Run2 increased by 9% in Run2, and the amount of the consumed CH_3CHO increased by 3%, leading to a 10% increase in the O_3 concentration at 6 h.

In recent years, some studies have found that the photolysis reaction (R2) of nitric acid or nitrate adsorbed on the surface of natural and artificial materials may be an important source of HONO in the atmospheric environment, which is 1–3 orders of magnitude higher than that in the gas or liquid phase (Baergen and Donaldson, 2013; Ye et al., 2016, 2019). In the simulation of Run1 and Run2, the photolysis process of HNO_3 adsorbed on the reactor surface was treated the same as that in the gas phase, which may lead to a difference between the simulated and measured results. Thus, reaction R2 was added to the original MCM v3.3.1 (without R1) and then the simulation was re-conducted (Run3). In order to determine the maximum effect of reaction R2 on the results, the photolysis rate constant used for R2 was taken to be 3 orders of magnitude higher than that in the gas phase.

$$\mathrm{HNO_{3(surface)}}+h\nu \rightarrow \mathrm{HONO}+\mathrm{O}\left(^3\mathrm{P}\right). \quad \text{(R2)}$$

Compared with Run1, under low-RH conditions, the simulated O_3 concentrations at 6 h for $R_{CN} \leqslant 3.4$ in Run3 increased by 4%–8%, while for $R_{CN} \geqslant 4.6$, they increased by only 1%–3%. Nevertheless, under high-RH conditions, the simulated O_3 concentrations at 6 h for $R_{CN} \leqslant 3.0$ in Run3 increased by 5%–13%, but for $R_{CN} \geqslant 6.7$, they increased by only 1%–2%. Compared with Run1, the Run3-simulated NO_y concentrations at 6 h only increased by 8% and 6% on average in Expts. 1–8 and Expts. 9–14, respectively. The Run3-simulated CH_3CHO concentrations at 6 h are 6% ± 19% and 9% ± 6% higher than the measured results in Expts. 1–8 and Expts. 9–14, respectively, which are also close to those between Run1-simulated results and experiments (5% ± 15% and 10% ± 6% in Expts. 1–8 and Expts. 9–14) (Figs. 6e and 6f). Therefore, compared with the Run1-simulated results, the results of NO_y and O_3 are improved to some extent under different reaction conditions.

As discussed above, compared with the Run1-simulated results, the increase of O_3 in Run2 was generally larger than that in Run3, which may be due to the effect of HNO_3 concentration on the reactor surface. Because the effect of R2 on the reaction increases with the increase of the HNO_3 concentration on the reactor surface, in the early stage of the reaction, the low content of HNO_3 on the reactor surface led to the small effect of R2 on the reaction. Taking Expt. 2 as an example, compared with the simulation results in Run1, the OH radical concentration at 3 h increased by 11% in Run3, while it increased by 28% at 6 h. Under high R_{CN}, the content of HNO_3 on the reactor surface is lower than that under low R_{CN}. Thus, after R2 was

added into the MCM, the increase for O_3 under high R_{CN} is smaller than that under low R_{CN}.

Because both reactions R1 and R2 can affect the conversion of NO_x, there may be interactions between R1 and R2 in the reaction. In order to determine the influence of the interaction between R1 and R2 on the simulated results, both R1 and R2 were added into the original MCM v3.3.1 for re-simulation (Run4) (Fig. 6). Under low-RH conditions (Expts. 1–8), the simulated O_3 concentrations at 6 h in Run4 increased by 14%–23% as compared with those in Run1 for $R_{CN} \leqslant 3.4$, while they displayed an increase of 5%–10% for $R_{CN} \geqslant 4.6$ (Fig. 6a). Similarly, under high-RH conditions (Expts. 9–14), compared with Run1, the simulated O_3 concentrations at 6 h in Run4 increased by 13%–21% and 6%–9% for $R_{CN} \leqslant 3.0$ and $R_{CN} \geqslant 6.7$, respectively (Fig. 6b). On the whole, the differences in O_3 concentrations at 6 h between simulations and experiments are greatly reduced from 24%–35% and 17%–49% in Run1 to 6%–26% and 10%–42% in Run4 for low- and high-RH experiments, respectively. This demonstrates that the inclusion of both R1 and R2 in MCM can greatly improve the simulation of O_3 by 13%–74%, relative to original MCM. Meanwhile, compared with the Run1-simulated IR_{6h}, Run4-simulated results of IR_{6h} increased by 12% ± 8% and 14% ± 7% in Expts. 1–8 and Expts. 9–14, respectively (Figs. 6g and 6h).

It is known from the simulated O_3 concentrations that the combined effect of R1 and R2 is clearly greater than that of R1 or R2 alone and is nearly equal to the total effect of the sum of R1 and R2 in some experiments. Taking Expt. 2 as an example, compared with Run1, the addition of R1 into original MCM (Run2) reduced the concentration of PAN at 6 h by 1.2%, but increased the concentration of HNO_3 on the reactor surface at 6 h by 4.0%, which increased the O_3 concentration at 6 h by 10.4%. After adding R2 into original MCM (Run3), the HNO_3 on the reactor surface at 6 h reduces by 69.1%, but the PAN concentration at 6 h increased by 15.8%, leading to the increase of the O_3 concentration at 6 h by 8.4%. After adding R2 and R3 into original MCM (Run4), the HNO_3 on the reactor surface at 6 h reduced by 67.9%, but the PAN concentration at 6 h increased by 15.0%. As a result, the O_3 concentration at 6 h increased by 19.7%. Therefore, when R1 and R2 exist at the same time, their effects on the O_3 concentration are close to the total effect of the sum of R1 and R2.

In order to see whether MCM can accurately determine the inflection point of variation of the O_3 concentrations at 6 h with R_{CN}, the MCM mechanisms used in Runs1–4 above were used to simulate the O_3 concentrations at 6 h (CH_3CHO = 600 ppb). Under the conditions of RH = 12%, the R_{CN} at the inflexion points in Runs1–4 was found to be 2.4, 2.2, 1.8 and 2.1, respectively (Fig. 7). Obviously, the simulation that is closest to the fitting result in Expts. 1–8 (R_{CN} = 3.2) is Run1, followed by Run2, Run4 and Run3. Under the condition of RH = 78%, the R_{CN} at the inflexion points in Runs1–4 is 4.8, 4.6, 4.1 and 4.0, respectively, while it is 2.8 from the fitting result in Expts. 9–14. Therefore, the modified MCM can improve the simulation of R_{CN} at the inflection point under high-RH conditions while it can worsen the simulation under low-RH conditions. In addition, the simulated results in Runs1–4 also show that the effects of RH on the O_3 concentrations under high R_{CN} are larger than those under low R_{CN}, which is in agreement with experimental results.

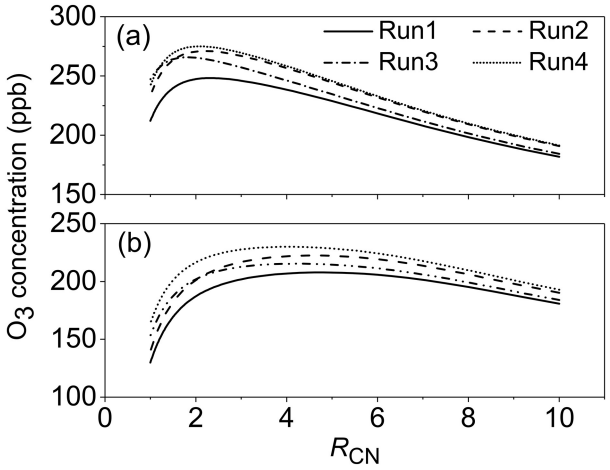

Fig. 7. Variations of simulated O_3 concentrations at 6 h by MCM mechanism with R_{CN} (CH_3CHO = 600 ppb, T = 300 K; a: RH = 12%; b: RH = 78%; Run1: original MCM v3.3.1; Run2: MCM v3.3.1 with R1; Run3: MCM v3.3.1 with R2; Run4: MCM v3.3.1 with R1 and R2).

3.3. *Ozone formation potential of CH_3CHO*

The ozone concentration at 6 h is generally used to represent the actual ozone formation ability of VOC under typical sunlight irradiations, while the maximum ozone concentration is used to represent the ozone formation potential (Carter et al., 1993). The modified MCM with R1 and R2 was used to simulate the O_3 concentrations generated by 6 h of photochemical reactions of acetaldehyde under different concentrations of CH_3CHO and NO_2. The results are shown in Fig. 8a and Table 2. It can be estimated that in Fig. 8a, the R_{CN} value at the ridge of the ozone isolines is about 1.7, which indicates that in the regime of $R_{CN} < 1.7$, the formation process of O_3 by acetaldehyde photochemistry is sensitive to CH_3CHO, while in the regime of $R_{CN} > 1.7$, O_3 is under the NO_x -sensitive condition. In Expts. 9–14, the R_{CN} value at the inflection point of the O_3 concentrations at 6 h is about 2.8 (Fig. 2). This demonstrates that the modified MCM still underestimates the experiment-based R_{CN} by 39%.

It is known from the simulation results that under different scenarios the contribution of acetaldehyde to ozone is very different (Fig. 8a). For example, under the scenario of NO_2 = 50–200 ppb, CH_3CHO = 20–200 ppb, acetaldehyde can contribute 16–416 ppb O_3, whereas under the scenario of NO_2 = 30–50 ppb, CH_3CHO = 10–20 ppb, acetaldehyde can contribute 18–55 ppb O_3, which indicates that the contribution of acetaldehyde to ozone can still increase with the concurrent decrease of NO_2 and acetaldehyde concentrations. However, under the scenario of $NO_2 \leqslant 10$ ppb, $CH_3CHO \leqslant$

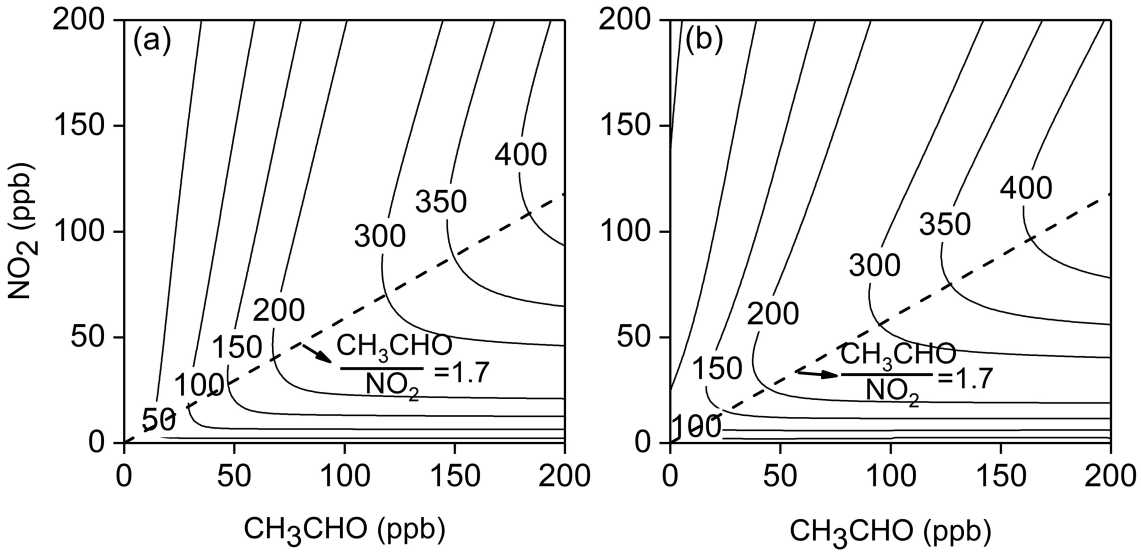

Fig. 8. Isogram of simulated O_3 concentrations after 6 h-photochemical reactions (RH = 70%, $J[NO_2]$ = 0.56 min^{-1}, T = 300 K; (a) acetaldehyde as a single VOC; (b) acetaldehyde plus other 11 species of VOCs: *m*/*p*-xylene = 1.6 ppb, propylene = 1.2 ppb, ethylene = 1.5 ppb, isoprene = 1.0 ppb, toluene = 2.4 ppb, 1-butene = 0.5 ppb, *o*-xylene = 0.6 ppb, isopentane = 2.2 ppb, 1,2,4-thrimethylbenzene = 0.3 ppb, *n*-butane = 2.7 ppb). The dashed line indicates the transition from CH_3CHO-sensitive to NO_x-sensitive conditions.

Table 2. Simulated results for different scenarios and background conditions. ([a]: Contribution of acetaldehyde to O_3 at 6 h, with deduction of the background O_3 concentration. [b]: The values in brackets indicate that the reactions of other VOCs have been added to the simulation as the background conditions, and the initial concentrations of other VOCs: *m*/*p*-xylene = 1.6 ppb, propylene = 1.2 ppb, ethylene = 1.5 ppb, isoprene = 1.0 ppb, toluene = 2.4 ppb, 1-butene = 0.5 ppb, *o*-xylene = 0.6 ppb, isopentane = 2.2 ppb, 1,2,4-thrimethylbenzene = 0.3 ppb, *n*-butane = 2.7 ppb.).

NO_2 (ppb)	CH_3CHO (ppb)	$O_{3\ 6h}$[a] (ppb)	IR_{6h} (ppb ppb^{-1})	MIR (ppb ppb^{-1})
50–200	20–200	16–416 (24–380)[b]	1.6–3.3 (1.3–3.6)[b]	3.9 (6.4)[b]
30–50	10–20	18–55 (32–70)[b]	3.0–3.4 (3.4–4.0)[b]	3.9 (4.4)[b]
⩽10	⩽2	1–7 (1–4)[b]	3.2–3.8 (0.5–1.8)[b]	4.0 (1.8)[b]

2 ppb, acetaldehyde can only contribute 1–7 ppb O_3.

In the actual atmospheric environment, there are many other kinds of VOCs that can affect the photochemical reaction of acetaldehyde and NO_x. For example, under the conditions of CH_3CHO = 2 ppb and NO_2 = 40 ppb, it is calculated that the O_3 concentration after 6-h reaction is 17 ppb. When the background air contains 1.6 ppb *m*-xylene, which was measured in the actual urban environment (Li et al., 2020), it can be calculated that the O_3 concentrations after 6-h reaction are 20 ppb and 24 ppb under the CH_3CHO concentrations of 0 and 2 ppb (NO_2 = 40 ppb), respectively, indicating that the ozone formation potential of *m*-xylene is larger than that of acetaldehyde, and that the existence of *m*-xylene greatly reduces the contribution of acetaldehyde to ozone. In order to analyze the sensitivity of O_3 formation to the acetaldehyde concentration in the actual atmospheric environment, we selected 11 species of VOCs with large contributions to the O_3 concentration in urban areas in the study of Li et al.(2020) as the background condition for the photochemical reaction of acetaldehyde. The simulated results are shown in Fig. 8b and Table 2. It is found that when the acetaldehyde concentration is much lower than the background VOCs (e.g., $CH_3CHO \leqslant 2$), because the reactions of background VOCs with OH radicals are dominant relative to acetaldehyde, background VOCs will weaken the contribution of acetaldehyde to O_3. When CH_3CHO = 10–20 ppb, NO_2 = 30–50 ppb, because the reaction of acetaldehyde with OH radicals is dominant or comparable relative to the background VOCs, and O_3 formation is mainly VOC-limited, background VOCs will enhance the contribution of acetaldehyde to ozone. When the acetaldehyde concentration is much larger than those of background VOCs, the effect of background VOCs on the photochemical reaction of acetaldehyde depends on the actual ratio of VOCs to NO_2. Indeed, in the actual environment, since the acetaldehyde concentration is much lower than those of background VOCs, it is considered that other VOCs will weaken the O_3 formation by the photochemical reaction of acetaldehyde in the actual environment.

The IR values of acetaldehyde under different reaction conditions (RH = 70%, T = 300 K) were simulated by using the modified MCM and Eq. (1) in this study. Taking the O_3 concentrations at 6 h, the IR_{6h} values were computed, and the results are shown in Fig. 9a. In addition, the maximum

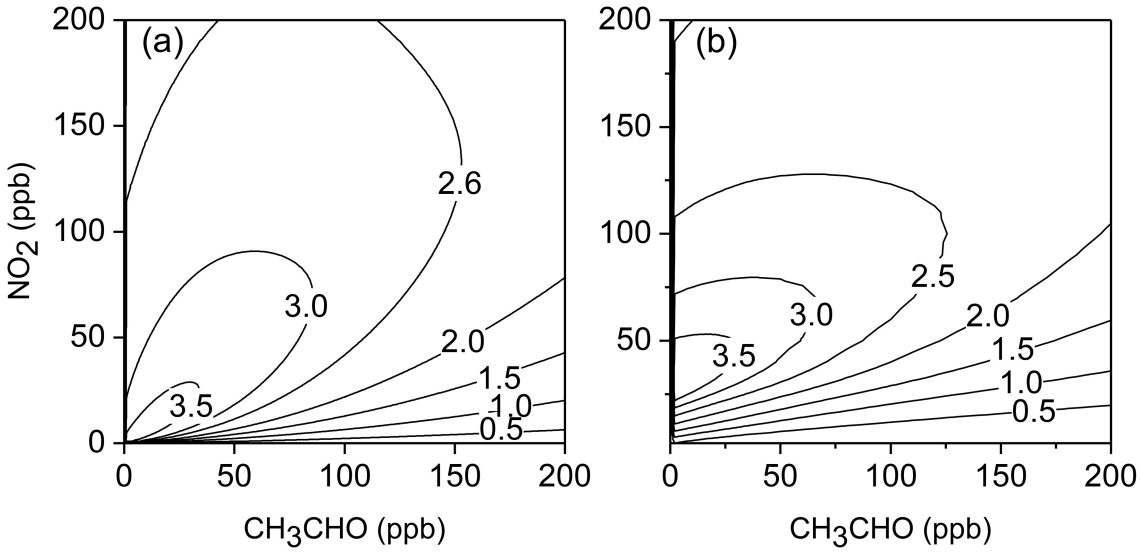

Fig. 9. Isogram of simulated IR at 6 h (RH = 70%, $J[NO_2]$ = 0.56 min^{-1}, T = 300 K; (a) acetaldehyde as a single VOC; (b) acetaldehyde plus other 11 species of VOCs: *m*/*p*-xylene = 1.6 ppb, propylene = 1.2 ppb, ethylene = 1.5 ppb, isoprene = 1.0 ppb, toluene = 2.4 ppb, 1-butene = 0.5 ppb, *o*-xylene = 0.6 ppb, isopentane = 2.2 ppb, 1,2,4-trimethylbenzene = 0.3 ppb, *n*-butane = 2.7 ppb).

incremental reactivity (MIR) was also simulated according to the maximum O_3 concentration under different scenarios (Table 2). The simulated results indicate that the MIR of acetaldehyde from the modified MCM is 4.0 ppb ppb^{-1}, which is 23% lower than the MIR value computed by Carter (2010) using the SAPRC-07 mechanism (RH = 50%, T = 300 K).

Similarly, to illustrate the effects of other VOCs on the IR value of acetaldehyde in the actual environment, the 11 species of VOCs were also added into the simulation of MCM as the background condition (Fig. 9b). It is found that the variation of IR_{6h} is similar to the variation of O_3 concentration before and after adding background VOCs. The IR_{6h} value of acetaldehyde will decrease under $CH_3CHO \leqslant 2$ ppb and $NO_2 \leqslant 10$ ppb, but it will increase when CH_3CHO = 10–20 ppb and NO_2 = 30–50 ppb. Nevertheless, when CH_3CHO = 20–200 ppb and NO_2 = 50–200 ppb, the variation of IR_{6h} depends on the actual ratio of VOCs to NO_2. Therefore, when the IR value is used to estimate the O_3 formation by acetaldehyde, the IR value should be selected according to the actual environmental conditions.

It is known from the MIR of acetaldehyde that acetaldehyde has an intermediate ozone formation potential. As estimated by Carter (2010), some species have high MIR values, such as methylglyoxal (22.2 ppb ppb^{-1}) and *m*/*p*-xylene (14.6/18.1 ppb ppb^{-1}), while some species have low MIR, such as benzene (0.68 ppb ppb^{-1}) and acetylene (0.27 ppb ppb^{-1}). If the difference in IR_{6h} between our simulation and experiments is taken into account, our MIR of acetaldehyde is underestimated by 25%. Thus, actual MIR of acetaldehyde should be 5.0 ppb ppb^{-1}, which is close to the value proposed by Carter (2010) (5.2 ppb ppb^{-1}). In this way, the MIR of acetaldehyde is probably between that of formaldehyde (4.5 ppb ppb^{-1}) and isobutene (6.2 ppb ppb^{-1}).

To estimate the role of acetaldehyde in the formation of O_3 in terms of MIR, the acetaldehyde concentration in the atmosphere is required. In Beijing of China, the concentration of acetaldehyde can reach about 5 ppb (Gu et al, 2019). In Sao Paulo megacity of Brazil, the concentration of acetaldehyde can reach about 10 ppb (Dominutti et al., 2020), while in the port megacity of Istanbul of Turkey, it can even reach about 15 ppb (Thera et al., 2019). Therefore, the contribution of acetaldehyde to ozone formation potential can be 25–75 ppb according to the MIR of acetaldehyde, which is an important precursor of ozone.

4. Conclusion

The photochemical reaction processes of CH_3CHO-NO_x have been studied in detail by smog chamber experiments and simulated by the MCM mechanism. The experiment results show that the R_{CN} has a significant effect on the concentrations of O_3 in the reaction process. In the low-RH experiments (RH = 11.6%±1.1%), when $R_{CN} < 3.2$, the O_3 concentration at 6 h increases with the increase of R_{CN}, while it decreases with the increase of R_{CN} when $R_{CN} > 3.2$. Similarly, the R_{CN} at the inflexion point of the change of O_3 concentration at 6 h is 2.8 in high RH experiments (RH = 78.8%±1.0%). Under low R_{CN} (< 3), RH has no significant effect on the O_3 concentrations, but under high R_{CN} (> 3), the O_3 concentrations at 6 h in the high-RH experiments were 16% lower than those in the low-RH experiments on average. Original MCM v3.3.1-simulated results of O_3 concentrations at 6 h are much smaller than those from the low- and high-RH experiments. After adding both the photolysis process of PAN and the photolysis process of HNO_3 on the reactor surface into the original MCM, the difference between the simulated O_3 concentrations by MCM and the

experimental results at the end of experiments reduced from 24%–35% and 17%–49% to 6%–26% and 10%–42% under low- and high-RH experiments, respectively. The current MCM mechanism of acetaldehyde underestimates the ozone generation potential of acetaldehyde, and the simulated MIR of acetaldehyde with the modified MCM mechanism is 4.0 ppb ppb^{-1} without considering the effects of other VOCs. When other 11 typical VOCs are included into the simulation of ozone as a background condition, the MIR value of acetaldehyde increased to 6.4 ppb ppb^{-1}. This demonstrates that acetaldehyde is probably an important precursor for ozone in the troposphere.

Acknowledgements. This work was supported by the National Key R&D Program of China (2017YFC0210005), the National Natural Science Foundation of China (Nos. 41875163, 41875166 and 41375129).

REFERENCES

Baergen, A. M., and D. J. Donaldson, 2013: Photochemical renoxification of nitric acid on real urban grime. *Environmental Science & Technology*, **47**(2), 815–820, https://doi.org/10.1021/es3037862.

Cao, Y. F., X. Qiao, P. K. Hopke, Q. Ying, Y. Y. Zhang, Y. Y. Zeng, Y. P. Yuan, and Y. Tang, 2020: Ozone pollution in the west China rain zone and its adjacent regions, southwestern China: Concentrations, ecological risk, and sources. *Chemosphere*, **256**, 127008, https://doi.org/10.1016/j.chemosphere.2020.127008.

Carter, W. P. L., 2010: Development of the SAPRC-07 chemical mechanism. *Atmos. Environ.*, **44**(40), 5324–5335, https://doi.org/10.1016/j.atmosenv.2010.01.026.

Carter, W. P. L., and G. Heo, 2013: Development of revised SAPRC aromatics mechanisms. *Atmos. Environ.*, **77**, 404–414, https://doi.org/10.1016/j.atmosenv.2013.05.021.

Carter, W. P. L., D. M. Luo, I. L. Malkina, and J. A. Pirece, 1993: An experimental and modeling study of the photochemical ozone reactivity of acetone. Final report to chemical manufacturers association contract No. KET-ACE-CRC-2.0, 43 pp.

Carter, W. P. L., J. A. Pierce, D. M. Luo, and I. L. Malkina, 1995: Environmental chamber study of maximum incremental reactivities of volatile organic compounds. *Atmos. Environ.*, **29**(18), 2499–2511, https://doi.org/10.1016/1352-2310(95)00149-S.

Chen, L. H., and Coauthors, 2020: The effects of humidity and ammonia on the chemical composition of secondary aerosols from toluene/NO_x photo-oxidation. *Science of The Total Environment*, **728**, 138671, https://doi.org/10.1016/j.scitotenv.2020.138671.

Chi, X. Y., and Coauthors, 2018: Observations of ozone vertical profiles and corresponding precursors in the low troposphere in Beijing, China. *Atmospheric Research*, **213**, 224–235, https://doi.org/10.1016/j.atmosres.2018.06.012.

da Silva, D. B. N., E. M. Martins, and S. M. Corrêa, 2016: Role of carbonyls and aromatics in the formation of tropospheric ozone in Rio de Janeiro, Brazil. *Environmental Monitoring and Assessment*, **188**(5), 289, https://doi.org/10.1007/s10661-016-5278-3.

Derwent, R. G., M. E. Jenkin, S. M. Saunders, and M. J. Pilling, 1998: Photochemical ozone creation potentials for organic compounds in northwest Europe calculated with a master chemical mechanism. *Atmos. Environ.*, **32**(14-15), 2429–2441, https://doi.org/10.1016/S1352-2310(98)00053-3.

Derwent, R. G., M. E. Jenkin, N. R. Passant, and M. J. Pilling, 2007: Photochemical ozone creation potentials (POCPs) for different emission sources of organic compounds under European conditions estimated with a Master Chemical Mechanism. *Atmos. Environ.*, **41**(12), 2570–2579, https://doi.org/10.1016/j.atmosenv.2006.11.019.

Dominutti, P., T. Nogueira, A. Fornaro, and A. Borbon, 2020: One decade of VOCs measurements in Sao Paulo megacity: Composition, variability, and emission evaluation in a biofuel usage context. *Science of The Total Environment*, **738**, 139790, https://doi.org/10.1016/j.scitotenv.2020.139790.

Dong, D., M. Shao, Y. Li, S. H. Lu, Y. J. Wang, Z. Ji, and D. G. Tang, 2014: Carbonyl emissions from heavy-duty diesel vehicle exhaust in China and the contribution to ozone formation potential. *Journal of Environmental Sciences*, **26**(1), 122–128, https://doi.org/10.1016/S1001-0742(13)60387-3.

Dong, Y. M., J. Li, J. P. Guo, Z. J. Jiang, Y. Q. Chu, L. Chang, Y. Yang, and H. Liao, 2020: The impact of synoptic patterns on summertime ozone pollution in the North China Plain. *Science of The Total Environment*, **735**, 139559, https://doi.org/10.1016/j.scitotenv.2020.139559.

Flowers, B. A., J. F. Stanton, and W. R. Simpson, 2007: Wavelength dependence of nitrate radical quantum yield from peroxyacetyl nitrate photolysis: Experimental and theoretical studies. *The Journal of Physical Chemistry A*, **111**(45), 11 602–11 607, https://doi.org/10.1021/jp0749118.

Gu, Y. Y., and Coauthors, 2019: Emission characteristics of 99 NMVOCs in different seasonal days and the relationship with air quality parameters in Beijing, China. *Ecotoxicology and Environmental Safety*, **169**, 797–806, https://doi.org/10.1016/j.ecoenv.2018.11.091.

Guérette, E. A., and Coauthors, 2020: Evaluation of regional air quality models over Sydney, Australia: Part 2, Comparison of $PM_{2.5}$ and ozone. *Atmosphere*, **11**(3), 233, https://doi.org/10.3390/atmos11030233.

Guo, S. J., X. L. He, M. Chen, J. H. Tan, and Y. H. Wang, 2014: Photochemical production of atmospheric carbonyls in a rural area in southern China. *Archives of Environmental Contamination and Toxicology*, **66**(4), 594–605, https://doi.org/10.1007/s00244-014-0013-y.

Hu, G. S., Y. F. Xu, and L. Jia, 2011: Effects of relative humidity on the characterization of a photochemical smog chamber. *Journal of Environmental Sciences*, **23**(12), 2013–2018, https://doi.org/10.1016/S1001-0742(10)60665-1.

Janik, R., M. Kubov, and B. Schieber, 2020: The ground-level ozone concentration in beech (*Fagus sylvatica* L.) forests in the West Carpathian Mountains. *Environmental Monitoring and Assessment*, **192**(4), 233, https://doi.org/10.1007/s10661-020-8176-7.

Jenkin, M. E., S. M. Saunders, and M. J. Pilling, 1997: The tropospheric degradation of volatile organic compounds: A protocol for mechanism development. *Atmos. Environ.*, **31**(1), 81–104, https://doi.org/10.1016/S1352-2310(96)00105-7.

Jenkin, M. E., S. M. Saunders, V. Wagner, and M. J. Pilling, 2003: Protocol for the development of the Master Chemical Mechanism, MCM v3 (Part B): Tropospheric degradation of aromatic volatile organic compounds. *Atmospheric Chemistry and Physics*, **3**, 181–193, https://doi.org/10.5194/acp-3-181-2003.

Jenkin, M. E., J. C. Young, and A. R. Rickard, 2015: The MCM v3.3.1 degradation scheme for isoprene. *Atmospheric Chemistry and Physics*, **15**(20), 11 433–11 459, https://doi.org/10.5194/acp-15-11433-2015.

Jia, L., 2007: A study of the kinetics of alkene ozonolysis and ozone formation reactivity of isopentane. M.S. thesis, Beijing Normal University. (in Chinese with English abstract)

Jia, L., and Y. F. Xu, 2016: Ozone and secondary organic aerosol formation from Ethylene-NO_x-NaCl irradiations under different relative humidity conditions. *Journal of Atmospheric Chemistry volume*, **73**(1), 81–100, https://doi.org/10.1007/s10874-015-9317-1.

Jia, L., and Y. F. Xu, 2018: Different roles of water in secondary organic aerosol formation from toluene and isoprene. *Atmospheric Chemistry and Physics*, **18**(11), 8137–8154, https://doi.org/10.5194/acp-18-8137-2018.

Jia, L., Y. F. Xu, M. F. Ge, L. Du, and G. S. Zhuang, 2009: Smog chamber studies of ozone formation potentials for isopentane. *Chinese Science Bulletin*, **54**(24), 4624–4632, https://doi.org/10.1007/s11434-009-0482-y.

Jia, L., Y. F. Xu, and Y. Z. Shi, 2011: Characterization of photochemical smog chamber and initial experiments. *Environmental Science*, **32**, 351–361. (in Chinese with English abstract)

Kalabokas, P., and Coauthors, 2020: A study of the influence of tropospheric subsidence on spring and summer surface ozone concentrations at the JRC Ispra station in northern Italy. *Atmospheric Chemistry and Physics*, **20**(4), 1861–1885, https://doi.org/10.5194/acp-20-1861-2020.

Kinose, Y., Y. Fukamachi, S. Okabe, H. Hiroshima, M. Watanabe, and T. Izuta, 2020: Toward an impact assessment of ozone on plant carbon fixation using a process-based plant growth model: A case study of *Fagus crenata* grown under different soil nutrient levels. *Science of The Total Environment*, **716**, 137008, https://doi.org/10.1016/j.scitotenv.2020.137008.

Li, Q. Q., and Coauthors, 2020: An investigation into the role of VOCs in SOA and ozone production in Beijing, China. *Science of The Total Environment*, **720**, 137536, https://doi.org/10.1016/j.scitotenv.2020.137536.

Liang, T. T., J. P. Niu, S. Y. Zhang, Q. Q. Song, and J. Zhou, 2020: Effects of high-temperature heat wave and ozone on hypertensive rats. *International Journal of Biometeorology*, **64**(7), 1039–1050, https://doi.org/10.1007/s00484-019-01788-w.

Libuda, H. G., and F. Zabel, 1995: Uv absorption cross sections of acetyl peroxynitrate and trifluoroacetyl peroxynitrate at 298 K. *Berichte der Bunsengesellschaft für physikalische Chemie*, **99**(10), 1205–1213, https://doi.org/10.1002/bbpc.199500061.

Luo, H., L. Jia, Q. Wan, T. C. An, and Y. J. Wang, 2019: Role of liquid water in the formation of O_3 and SOA particles from 1:2,3-trimethylbenzene. *Atmos. Environ.*, **217**, 116955, https://doi.org/10.1016/j.atmosenv.2019.116955.

Luo, H., G. Y. Li, J. Y. Chen, Y. J. Wang, and T. C. An, 2020: Reactor characterization and primary application of a state of art dual-reactor chamber in the investigation of atmospheric photochemical processes. *Journal of Environmental Sciences*, **98**, 161–168, https://doi.org/10.1016/j.jes.2020.05.021.

Ma, X. Y., H. L. Jia, T. Sha, J. L. An, and R. Tian, 2019: Spatial and seasonal characteristics of particulate matter and gaseous pollution in China: Implications for control policy. *Environmental Pollution*, **248**, 421–428, https://doi.org/10.1016/j.envpol.2019.02.038.

Saengsai, S., and W. Jinsart, 2015: Evaluation of urban ozone formation by photochemical ozone creation potential indices and generalized additive model. *Proc. Int. Conf. on Biological, Civil and Environmental Engineering*, Bali, Indonesia.

Seinfeld, J. H., and S. N. Pandis, 2006: *Atmospheric Chemistry and Physics: From Air Pollution to Climate Change*. 2nd ed. Wiley, 1149 pp.

Seltzer, K. M., D. T. Shindell, P. Kasibhatla, and C. S. Malley, 2020: Magnitude, trends, and impacts of ambient long-term ozone exposure in the United States from 2000 to 2015. *Atmospheric Chemistry and Physics*, **20**(3), 1757–1775, https://doi.org/10.5194/acp-20-1757-2020.

Shi, Y. Z., Y. F. Xu, and L. Jia, 2012: Development and application of atmospheric chemical mechanisms. *Climatic and Environmental Research*, **17**(1), 112–124, https://doi.org/10.3878/j.issn.1006-9585.2011.10061. (in Chinese with English abstract)

Talukdar, R. K., J. B. Burkholder, A. M. Schmoltner, J. M. Roberts, R. R. Wilson, and A. R. Ravishankara, 1995: Investigation of the loss processes for peroxyacetyl nitrate in the atmosphere: Uv photolysis and reaction with OH. *J. Geophys. Res.*, **100**(D7), 14 163–14 173, https://doi.org/10.1029/95JD00545.

Thera, B. T. P., and Coauthors, 2019: Composition and variability of gaseous organic pollution in the port megacity of Istanbul: Source attribution, emission ratios, and inventory evaluation. *Atmospheric Chemistry and Physics*, **19**(23), 15 131–15 156, https://doi.org/10.5194/acp-19-15131-2019.

Venecek, M. A., W. P. L. Carter, and M. J. Kleeman, 2018: Updating the SAPRC Maximum Incremental Reactivity (MIR) scale for the United States from 1988 to 2010. *Journal of the Air & Waste Management Association*, **68**(12), 1301–1316, https://doi.org/10.1080/10962247.2018.1498410.

Wang, T., L. K. Xue, P. Brimblecombe, Y. F. Lam, L. Li, and L. Zhang, 2017: Ozone pollution in China: A review of concentrations, meteorological influences, chemical precursors, and effects. *Science of The Total Environment*, **575**, 1582–1596, https://doi.org/10.1016/j.scitotenv.2016.10.081.

Wang, W. G., K. Li, L. Zhou, M. F. Ge, S. Q. Hou, S. R. Tong, Y. J. Mu, and L. Jia, 2015: Evaluation and application of dual-reactor chamber for studying atmospheric oxidation processes and mechanisms. *Acta Physico-Chimica Sinica*, **31**, 1251–1259, https://doi.org/10.3866/PKU.WHXB201504161.

Ye, C. X., H. L. Gao, N. Zhang, and X. L. Zhou, 2016: Photolysis of nitric acid and nitrate on natural and artificial surfaces. *Environmental Science & Technology*, **50**(7), 3530–3536, https://doi.org/10.1021/acs.est.5b05032.

Ye, C. X., N. Zhang, H. L. Gao, and X. L. Zhou, 2019: Matrix effect on surface-catalyzed photolysis of nitric acid. *Scientific Reports*, **9**, 4351, https://doi.org/10.1038/s41598-018-37973-x.

Zhao, T. Y., and Coauthors, 2020: Depression and anxiety with exposure to ozone and particulate matter: An epidemiological claims data analysis. *International Journal of Hygiene and Environmental Health*, **228**, 113562, https://doi.org/10.1016/j.ijheh.2020.113562.

Zong, R. H., L. K. Xue, T. Wang, and W. X. Wang, 2018: Intercomparison of the Regional Atmospheric Chemistry Mechanism (RACM2) and Master Chemical Mechanism (MCM) on the simulation of acetaldehyde. *Atmos. Environ.*, **186**, 144–149, https://doi.org/10.1016/j.atmosenv.2018.05.013.